An optical network of silicon micromachined sensors

Mark L. Wilson, David W. Burns, J. David Zook
Honeywell Technology Center
3660 Technology Drive, MN65-2600
Minneapolis, MN 55418
wilson_mark@htc.honeywell.com

Abstract

The Honeywell Technology Center, in collaboration with the University of Wisconsin and the Mobil Corporation, and under funding from this ARPA sponsored program, are developing a new type of "hybrid" micromachined silicon/fiber optic sensor that utilizes the best attributes of each technology. Fiber optics provide a noise free method to read out the sensor without electrical power required at the measurement point. Micromachined silicon sensor techniques provide a method to design many different types of sensors such as temperature, pressure, acceleration, or magnetic field strength and report the sensor data using FDM methods. Our polysilicon resonant microbeam structures have a built in Fabry-Perot interferometer that offers significant advantages over other configurations described in the literature. Because the interferometer is an integral part of the structure, the placement of the fiber becomes non-critical, and packaging issues become considerably simpler. The interferometer spacing are determined by the thin-film fabrication processes and therefore can be extremely well controlled. The main advantage, however, is the integral vacuum cavity that ensures high Q values. Testing results have demonstrated relaxed alignment tolerances in packaging these devices, with an excellent Signal to Noise Ratio (SNR). Networks of 16 or more sensors are currently being developed. STORM (Strain Transduction by Optomechanical Resonant Microbeams) sensors can also provide functionality and self calibration information which can be used to improve the overall system reliability. Details of the sensor and network design, as well as test results, are presented.

Keywords: fiber, optic, sensor, micromachined, silicon, MEMS, resonant, network

Introduction

The Honeywell Technology Center, in collaboration with the University of Wisconsin and the Mobil Corporation, is developing a new class of high-performance optical sensors. This work has been done under internal Honeywell research projects and also under contract funding sponsored by an ARPA/ARL program entitled "Optomechanical Resonant Sensor Modules for Multipoint Sensing". These optical sensors, henceforth called STORM sensors (Strain Transduction by Optomechanical Resonant Microbeams), represent a new and novel electromechanical sensor technology which combines the strength of silicon resonant micro-beam sensor technology including high sensitivity, stability, and robustness with those of optical fiber technology, including EMI immunity and intrinsic safety. STORM technology provides the generic basis for a wide range of sensors that offer significant advantages over conventional silicon only or fiber only sensors. In particular, STORM based sensor modules have great potential for multi-point distributed sensing, sensing of multiple parameters, and remote sensing in hostile environments. At the same time, they have excellent low cost potential, since fibers ultimately replace copper wiring.

The sensing element of a STORM sensor is a polysilicon microbeam attached at one or both ends. Figure 1 details the structure of the basic microbeam. The microbeam is free to vibrate in and out of the plane of the microbeam and is surrounded by a vacuum enclosure. The enclosure is fabricated monolithically and provides a vacuum environment for the microbeam to vibrate at its natural resonant frequency (100 KHz - 900 KHz) with relatively low losses and high Q. Each microbeam contains an embedded photodiode fabricated beneath the beam. A modulated laser input is used to illuminate the photodiode. This generates an electrostatic force that attracts the microbeam and drives the beam into

0-8194-2061-1/96/$6.00

resonance. The natural frequency of the STORM sensor is designed to be controlled by an external parameter, such as pressure or temperature, that the sensor is to monitor as detailed in Figure 1. Light reflected from the resonating sensor will be modulated at the resonant frequency and monitored externally. Multimode optical fibers will be used to route the drive and sense optical signals to and from the STORM device.

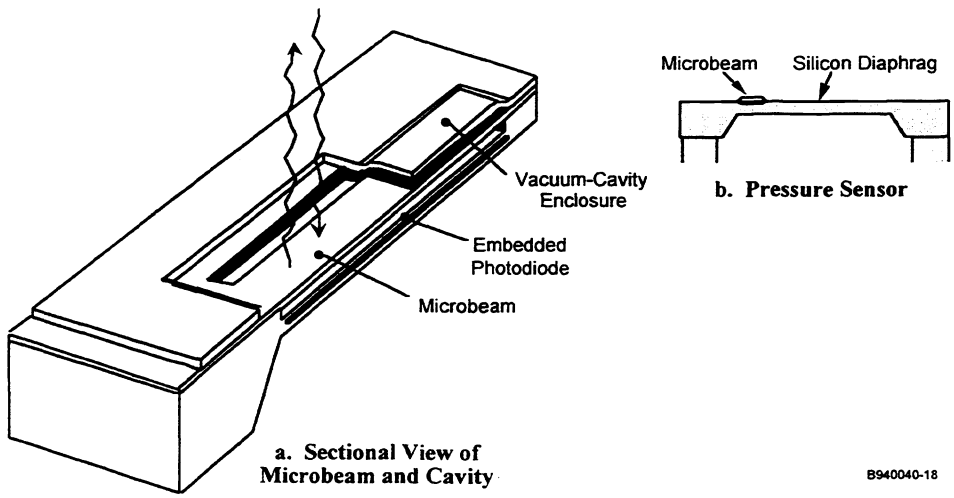

Figure 1. Cross section of STORM sensing element showing a rectangular polysilicon microbeam in a vacuum cavity enclosure. A photodiode is fabricated in the silicon underneath the microbeam to provide for optical excitation. Optical interference of light reflected off the vibrating microbeam causes modulation of the output signal at the resonant frequency of the microbeam. A pressure sensor using the optoelectromechanical transduction mechanism is illustrated in Figure 1b.

Sensor Design

The STORM sensors are unique compared to other fiber optic resonant sensors that have been described in the literature.[1-5] Venkatesh and Culshaw[1] first demonstrated optical excitation and sensing of a microresonator structure in 1985. In the devices described in the literature, the resonator movement is sensed by optical interference between the resonator and a close spaced optical fiber. Detailed analysis of this readout mechanism, of the optothermal excitation mechanism, and of the conditions for self-resonance have been given [3-5].

Our polysilicon resonant microbeam structures have a built-in Fabry-Perot interferometer that offers significant advantages over the configurations described in the literature. Because the interferometer is an integral part of the structure, the placement of the fiber becomes non-critical, and packaging issues become considerably simpler. The interferometer spacing are determined by the thin film fabrication processes and therefore can be extremely well controlled. The main advantage, however, is the integral vacuum cavity that ensures high Q values. The high Q means that very little energy is required to drive the beam at resonance.

A micrograph of a STORM device is shown in Figure 2. The resonating microbeam is attached to support posts at each end of the device. This entire structure is assembled inside a vacuum cavity formed as the numerous holes used for etching are sealed inside a vacuum deposition chamber. This basic device is fabricated on top of other microstructures that are designed to cause stress as a function of some external parameter such as temperature, pressure, or magnetic field strength. We have developed 16 element STORM sensor arrays each with a different length and a non-overlapping resonant frequency. This allows individual sensors to be addressed on a wide bandwidth network using Frequency Division Multiplexing (FDM) techniques.

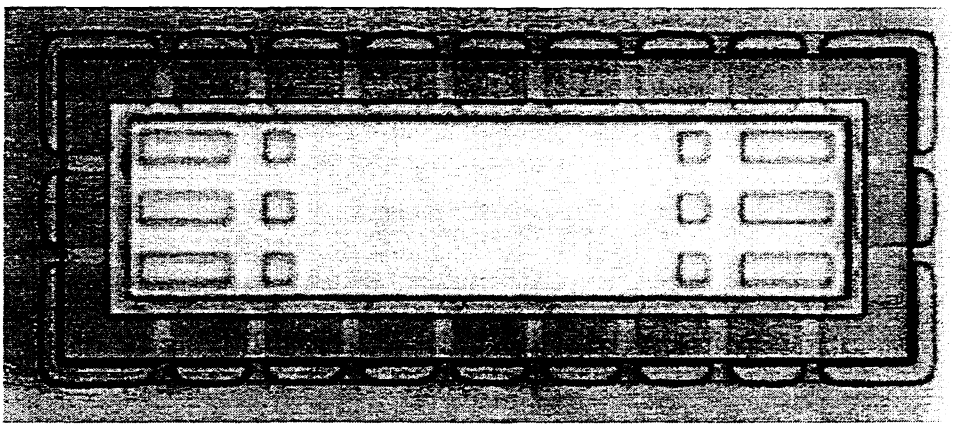

Figure 2: This is a micro-graph taken of an actual STORM device developed in our laboratory. This device has a span of about 100 μm between the set of support posts used to define the resonating beam's length. This structure is sealed inside a vacuum cavity to yield high Q devices.

Figure 3 is a plot detailing how the frequency of four separate beams on a single STORM chip vary as a function of temperature. Each of these individual STORM devices has a different length and thus a different resonant frequency. Each of these four beams have been designed such that their resonant frequencies never overlap within the temperature range that they were designed for. All of the beams have about the same sensitivity as a function of temperature. We have also developed devices that have 16 non-overlapping frequencies on a single silicon. This allows users of these sensors to maintain inventory in a single device rather that requiring the maintenance of 16 different sensors.

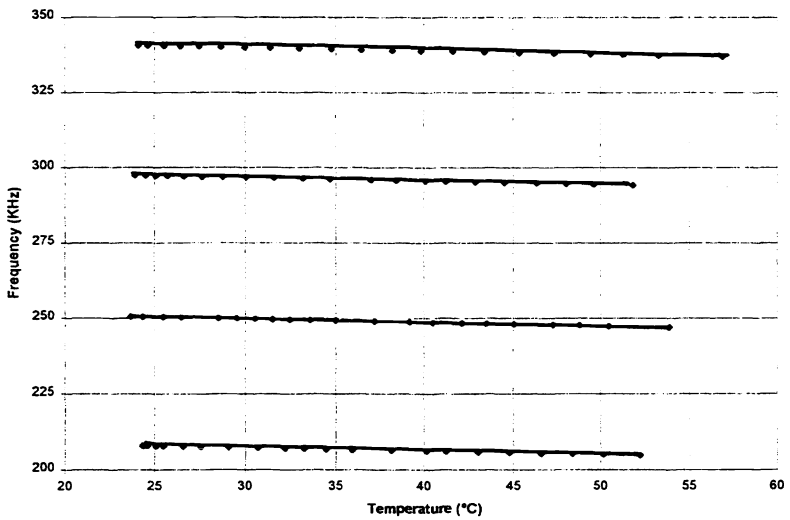

Figure 3: This figure illustrates the resonant frequency as a function of temperature for a single Storm chip with four separate resonators on it. Note that they have been designed to not overlap in frequency over a wide range of temperatures.

A schematic cross-section of a STORM sensor in its vacuum enclosure is shown in Figure 4. The incident light signal illuminates the internal photodiode which causes an electrostatic force on the microbeam. This force pulls the microbeam toward the photodiode. As the illumination supplied by the incident light beam is removed, the force acting on the microbeam is reduced and the microbeam relaxes. If the incident light beam is modulated at the resonant

frequency of the microbeam, it will resonate. The small physical movement of this beam causes a substantial modulation of the reflected light intensity because of constructive and destructive interference effects from multiple reflections off of the many different surfaces inside the device. The device acts as a microetalon.

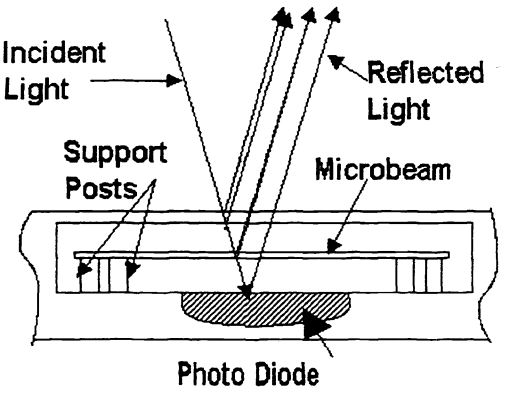

Figure 4. The light reflected off of the resonant microbeam and surrounding structure is the result of interference between the rays from the four internal surfaces. Movement of the microbeam causes modulation of the reflected light.

Reflections from the top of the polysilicon shell are made negligible by the use of an anti-reflective coating. The thickness of the cavities above and below the microbeam are chosen such that their sum is a half wave of the incident light, and the microbeam is chosen to be an odd multiple of a quarter-wave thickness. The reflectance of the structure as a function of position in the cavity is given in Figure 5. When the lower gap is zero or a multiple of a half-wave thick, the structure is anti-reflecting. When the lower gap is an odd multiple of a quarter wave thick, the reflectivity is twice the reflectivity of bare Silicon or about 66% at normal incidence. Multiple reflection effects give the structure Fabry-Perot-like characteristics with an effective finesse of about 3.7. For operation as an optomechanical modulator, the beam and gap thickness should be chosen to lie on the steep part of the curve where the change in reflectivity per unit displacement of the beam is maximized. With this choice of operating point, the modulation index of the reflected light will be close to 100% for a beam vibration amplitude of 1/8 wave, or about 100 nm.

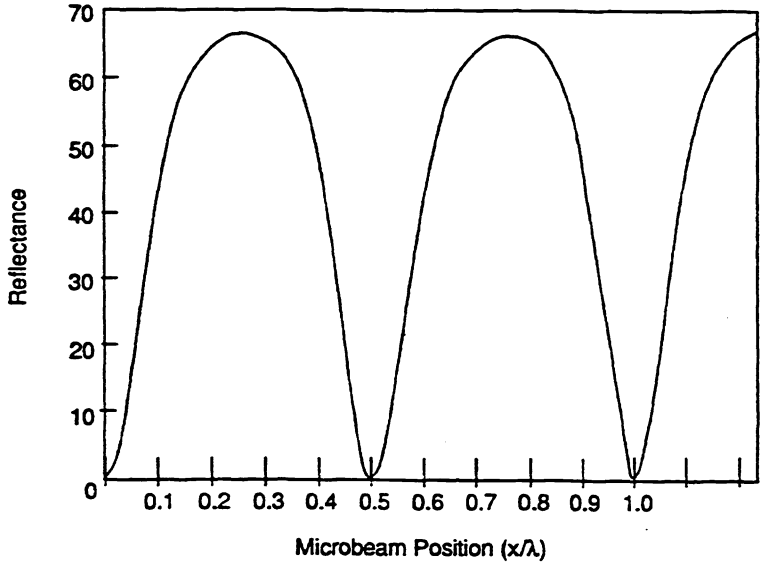

Figure 5. Calculated reflectivity of the structure of Figure 1 as a function of position of the microbeam within the enclosed cavity.

Network Design

Two different network topologies have been investigated to construct large networks of sensors connected to a central signal processor; one based upon a lightly tapped linear bus, and the second approach based upon a star bus. These designs are detailed in Figure 6 and 7. Figure 6 illustrates a lightly tapped linear bus network design. This network utilizes a single fiber to connect up several sensors. The mirror inside the sensor assembly could also be replaced with optical interference filters to allow the use of Wavelength Division Multiplexing (WDM) as well as FDM methods. Combining WDM and FDM techniques allows a larger number of sensors to be connected to the network.

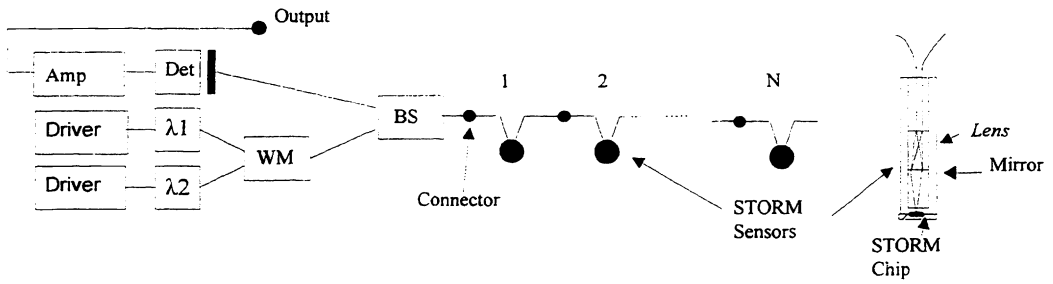

Figure 6. This block diagram details the construction of a lightly tapped linear bus network of STORM sensors. The structure of the sensor is also shown.

Figure 7 illustrates a STAR coupler network design topology. Each sensor has a single optical fiber attached to it which is used to route optical signals to and from the sensor. Each sensor ultimately connects up to a large NxN optical coupler which provides a direct but lossy path between each sensor and the signal processing system. It may be possible to reduce the loss of the star coupler approach by bundling several of the output fibers together into a single large area photo-diode.

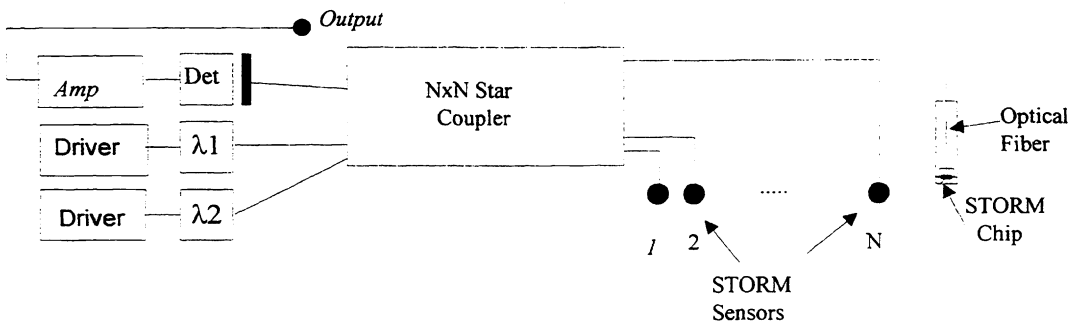

Figure 7. This block diagram details the construction of a star bus network of STORM sensors. The structure of the sensor is also shown.

The optical loss model was developed to help in the design of the STORM sensor network. This model allows the input optical power from the laser, the loss of various optical components, as well as loss from optical connectors and the STORM devices to be input to compute the overall performance of the network. Each parameter can be individually adjusted and take the form of transmission efficiencies. The loss model for the star bus approach is described by the following equation:

$$P_{SO} = P_{LA} \cdot \eta_{IN} \cdot \eta_{WM} \cdot \frac{\eta_{BS}^{\,2}}{N^2} \cdot (\eta_{CO} \cdot \eta_{LS})^2 \cdot \eta_{LS}^{\,2} \cdot \eta_{SS}$$

where

P_{SO}	=	Power of Nth sensor signal	
P_{LA}	=	Output power of the laser	10 mw
η_{IN}	=	Input coupling efficiency	.95
η_{WM}	=	Wavelength Multiplexer efficiency	.95
η_{BS}	=	Beamsplitter efficiency	.95
η_{CO}	=	Optical connector efficiency	.99
η_{LS}	=	Lens coupling efficiency	.99
η_{SS}	=	STORM sensor reflection efficiency	.20

Figures 8 is a plot which demonstrates how the signal power, drive power, and reflected power vary as a function of the number of sensors on each of the linear and star networks respectively. These plots are based upon the parameter values shown above which are optimistic but obtainable.

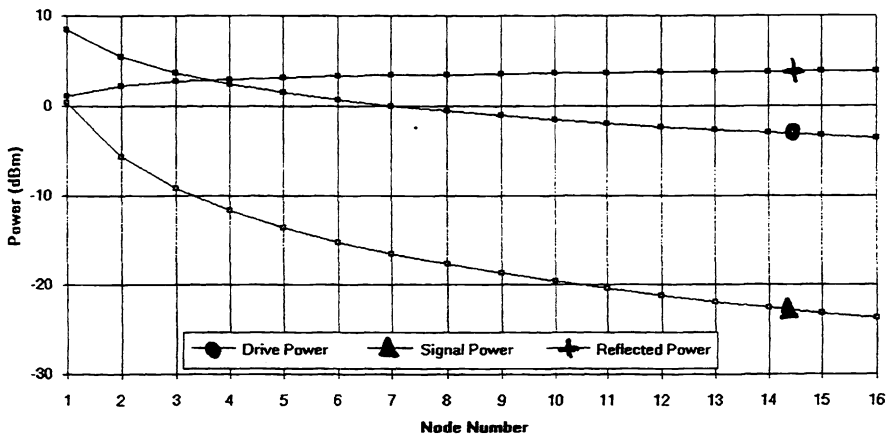

Figure 8. The drive power, signal power, and reflected power is shown as a function of the number of sensors on a star optical bus. The signal power of -25 dB for 16 sensors is well within the capability of optical receivers developed for fiber optic communications.

The advantage of a linear tapped bus is that a single fiber can be used to connect up the entire network. However, this can also be a disadvantage if the fiber is damaged or broken since all sensors down stream from the break would no longer function. The star bus has the advantage that the signal levels are higher and there is no single point failure mechanism except if the star coupler is damaged. A doubly redundant star could provide more fault tolerance but also doubles the network complexity.

The signal obtained from an actual STORM device is shown in Figure 9. This signal was obtained using a HP spectrum analyzer which was programmed to sweep a source signal through a 20 KHz span centered around 290 KHz. Note the noise floor is at -90 dBm, and the signal is about +45 dB above the noise floor. The Signal to Noise Ratio (SNR) of this signal is very large making signal processing much easier. In Figure 9, the spectrum analyzers filter bandwidth is convolved with this resonant peak, so the actual peak is much sharper that shown in this figure.

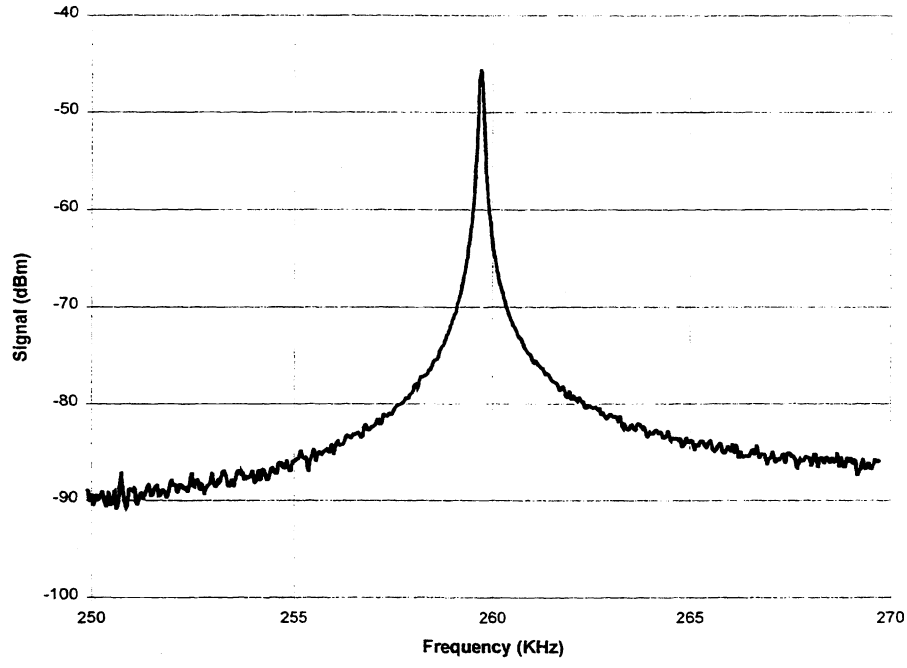

Figure 9: The resonant frequency spectrum of an actual STORM device is detailed in this figure.

Package Design and Testing

In order to develop a suitable package for the STORM sensors, we first established a series of designed experiments to determine the sensitivity of the sensors to packaging misalignments. A 6 axis micro-positioning packaging fixture was used to move the STORM device relative to the end of the optical fiber used to drive and sense the microbeam's resonance. First the lengthwise sensitivity was tested by visually placing the optical fiber just off the device, but in the X axis center. Then starting at one side of the device and moving across in 0.01 mm increments, the peak frequency and amplitude were recorded. Once this data was plotted, the X position with the most signal was used to test for the Y sensitivity. Again 0.01 mm increments were used to move across the beam to find the maximum signal. Once the X and Y sensitivity testing was completed, the Z axis testing was started. This consisted of a dial indictor reading the Z axis stage in 0.01 mm. The optical fiber was positioned just above the device, but not touching it. The Z stage was then moved down in 0.01 mm increments while recording the peak frequency and amplitude. The Z axis testing continued until the signal strength had diminished to zero.

Figure 10 illustrates the typical amplitude and frequency sensitivity to the position of the optical fiber with respect to the center of the STORM devices. The amplitude of the signal from the STORM device is virtually unaffected by the value of the X position (10a), however, the resonant frequency is strongly changed. There is a stable operational point at ±10 micron of the center of the device which has shifts in frequency less than 10 Hz. This level of packaging tolerance should make device packaging easier. Figure 10b details the widthwise (narrow direction) position results and Figure 10c is a plot of the Z axis position results for this STORM device. The reduction in amplitude of the signal with increased Z position was anticipated since the area illuminated by the diverging cone of light exiting the input optical fiber grows larger as Z increases, while the light collection area of the optical fiber is fixed. Thus the collected light signal should fall off as $\sim 1/Z^2$.

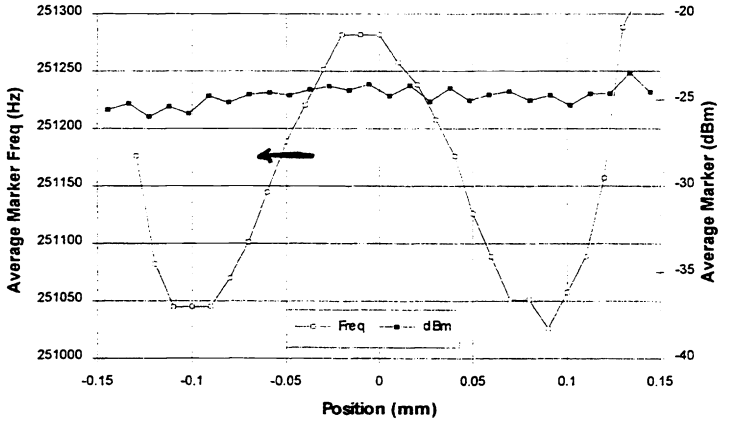

(a)

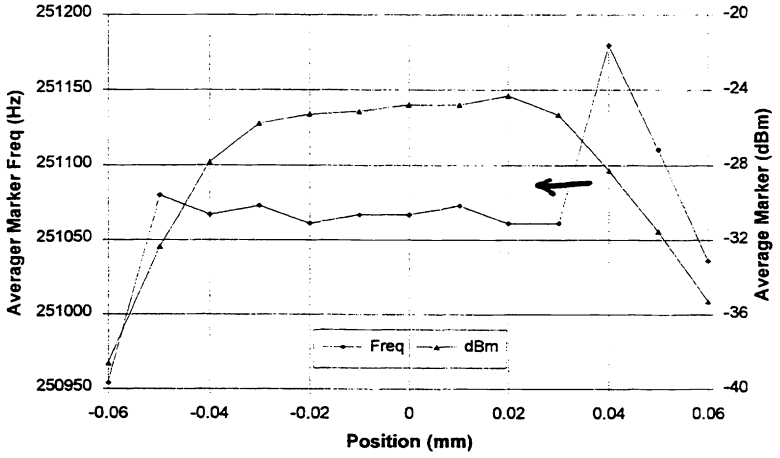

(b)

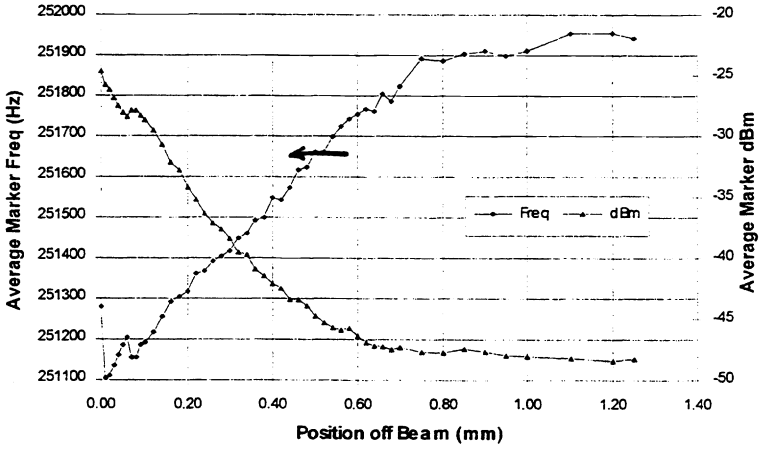

(c)

Figure 10. The effect of XYZ misalignments is detailed in this figure. The results are nearly identical to ones obtained from previous testing. (a=X=top, b=Y=middle, c=Z=bottom)

High order polynomial models were fitted to the XYZ data contained in Figure 10. From an RMS error analysis of these XYZ models, we determined that the resonant frequency of a device would undergo less than a 2 Hz shift if the end of the input fiber was miss-aligned by 1 micron in each of the 3 axis. Thus, our alignment tolerance for a 10 Hz accuracy device is several microns, which can be maintained with relative ease. The design of a temperature sensor package concept is shown in Figure 11. A glass tube containing an optical fiber at its center is attached to the STORM chip using adhesives or solders. This glass tube provide excellent stabilization of the end of the fiber with respect to the center of the STORM device, and also provide structural integrity to the STORM chip since the glass tube and silicon have similar thermal expansion coefficients.

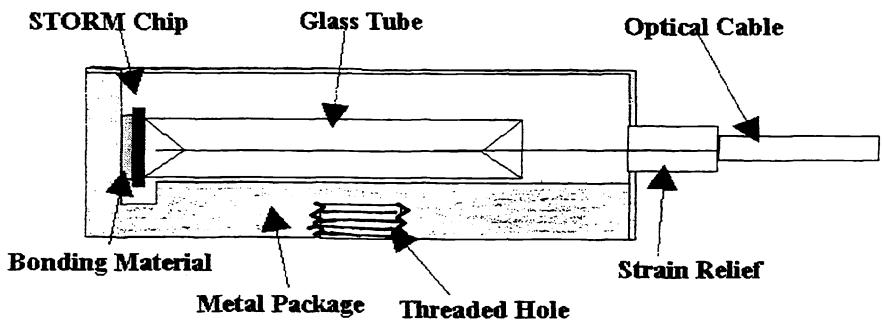

Figure 11: This is a drawing illustrating how the STORM sensors are packaged. A glass tube provides the connection between the optical fiber and the STORM chip. The tube is attached using adhesives or solder. Strain relief to the optical cable is provided by crimping the cable to the metal box used to surround and protect the optical components insider the package.

We have developed a fixture to assist in the packaging of our devices. This fixture uses a video camera and monitor to allow the operator to visually align the optical fiber with respect to the STORM device. Once the fiber is in position, the resonance of the STORM device is monitored by down mixing the high frequency of the device down to audio frequencies. The operator uses a speaker to listen to the down mixed resonance signal. When the fiber is correctly positioned in the XY plane, the frequency would be at a maximum. Similarly, when the fiber is correctly positioned along the Z axis, the frequency would be at a minimum. We expect that using the actual tones generated by the STORM device will provide an excellent way of actively aligning the sensor. An independent Z axis on the fiber alone is also provided to allow the operator to move the glass tube and fiber independently. The STORM chip is immobilized using a vacuum chuck. This vacuum chuck base can be electrically heated to 250°C so that solders or thermal set adhesives can be used to bond the fiber, glass tube, and silicon die together. The finished device is easily released by removing two small magnetic clamps. Current packages are 5x5x15 mm, but smaller packages are planned.

Signal Processor Design

A block diagram of the signal processor module design is shown in Figure 12. A direct digital synthesizer is used to create a low phase-noise sine wave that serves as a stimulus for the sensor. The rest of the system recovers the in-phase and quadrature components of the signal from the resonator. By examining both of these components, all of the information about the behavior of the resonator is acquired and may be manipulated mathematically to extract the magnitude and the phase angle.

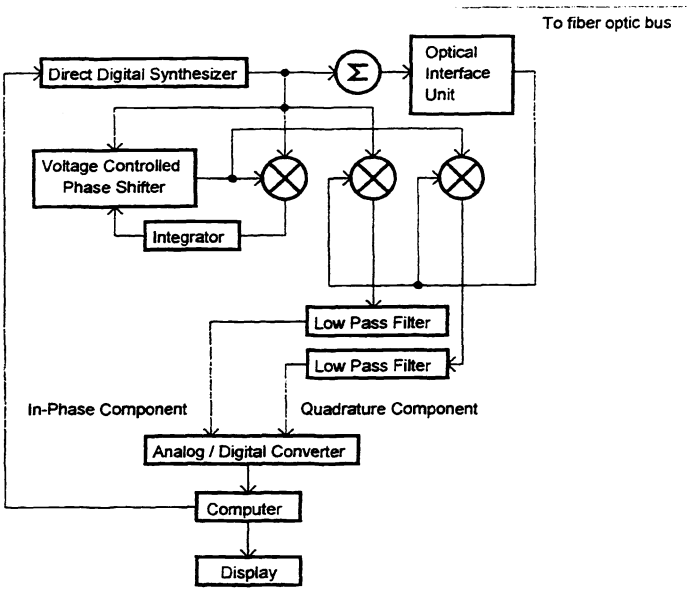

Figure 12: This is a diagram of the signal processor module as it is presently configured.

The overall system concept consisting of 16 STORM devices is shown in Figure 13. Each STORM device has a dedicated electronic circuit for resonance tracking. A fiber-optic star network connects the STORM devices to the sensor electronics. A digital I/O bus connects the sensor electronics to a notebook computer having a digital I/O card. The notebook computer displays various types of information about the system. Through a graphical user interface (GUI), the user can select what information to display and control the overall operation of the system.

The system software installed on the notebook computer will be developed using National Instrument's Lab Windows programming environment. Lab Windows allows development of complex process monitoring and control software, having sophisticated GUI displays, in a relatively short period of time. Furthermore, Lab Windows has interface programming tools for National Instrument's digital I/O cards, which can be used to interface the notebook computer to the sensor electronics

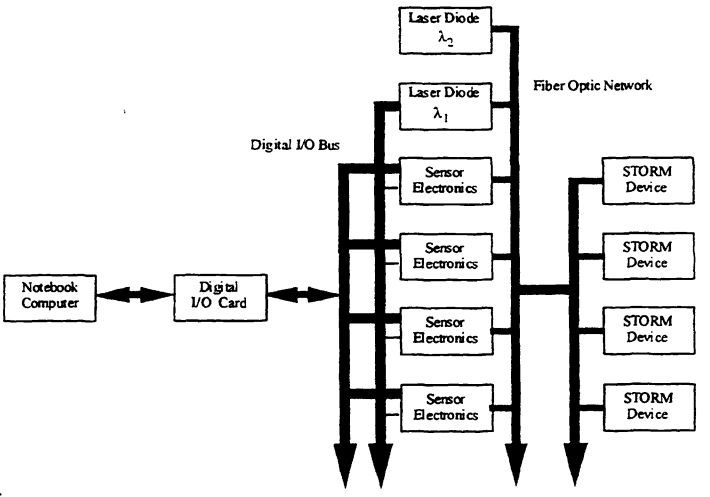

Figure 13. Block diagram of the STORM system consisting of 16 sensors.

Each STORM device has a dedicated electronics module that acquires and tracks its resonant frequency. All the electronics modules are identical, therefore capable of working with any STORM device. The user selects which electronic module is dedicated to which STORM device. The resonance frequencies of the STORM devices are communicated through the digital I/O bus to the notebook computer. Commands from the notebook computer can be sent to the electronics modules. These commands can initialize the electronics modules, facilitate the process of acquiring the resonance frequency of a STORM device, and provide error corrections to the tracking process.

Conclusion

We have developed a new type of "hybrid" micromachined silicon/fiber optic sensor that utilizes the best attributes of each technology. Fiber optics provide a nearly noise free method to read out the sensor without electrical power required at the measurement point. The micromachined silicon STORM devices provide a method to design many different types of sensors such as temperature, pressure, acceleration, or magnetic field strength and report the sensor data using FDM methods. Testing results have demonstrated relaxed alignment tolerance in packaging these devices with excellent SNR. Networks of 16 or more sensors are currently being developed. Finally, the STORM sensors provide functionality and self-calibration information which can be used to improve the overall system reliability.

Acknowledgments

A number of people have contributed significantly to the results discuss in this paper. Anis Husain and Kaigham Gabriel of ARPA have shown great foresight in realizing the potential of this technology by funding this research project under contract number DAAL01-94-C-3427. Richard Wittstruck from ARL/EDR has provided very valuable consultation on where to target this technology for both military and commercial applications, and has also been very understanding of the changes of direction of the project to date. Gerry Trenta and Ron Szanyi of Mobil Corporation have been very helpful in targeting commercial refinery applications of these sensors. Internally at Honeywell, Barry Cole, Bob Horning, Jerry Huber, Bob Martin, Dane Larson, Peg Wilson, and Bill Herb have provided valuable support in modeling, designing, and fabricating the STORM devices. We would also like to thank Henry Guckel from the University of Wisconsin for his pioneering research in micro-machined sensor technology, and for his many consultations on this work. Finally, Jerry Bolser, Ernie Satren, and Cindy Bassett have done an excellent job of designing test fixtures, providing test data, and packaging of the devices presented in this report. Thanks to all.

References

1. S. Venkatesh and B. Culshaw, "Optically activated vibration in a micromachined silica structure," *Electronics Letters,* **21,** pp. 315–7, 1985.

2. M.V. Andres, M.J. Tudor, and K.W.H. Foulds, "Analysis of an interferometric optical fiber detection technique applied to silicon vibrating sensors," *Electronics Letters,* **22**, pp. 1097–9, 1986.

3. M.J. Tudor, M.V. Andres, K.W.H. Foulds, and J.M. Naden, "Silicon resonator sensors: interrogation techniques and characteristics," *IEEE Proc.*, **135**, (Part D, No. 5), 1988.

4. N.A.D. Stokes, R.M.A. Fatah, and S. Venkatesh, "Self-excitation in fiber-optic microresonator sensors," *Sensors and Actuators,* **A21-23**, pp. 369–372, 1990.

5. A.V. Churenkov, "Photothermal excitation and self-resonance of silicon microresonators," *Sensors and Actuators* **A39,** pp141-148, 1993.